International Journal of
Intelligent Systems and Applications in Engineering

ISSN:2147-6799 www.ijisae.org Original Research Paper

A Dynamic AI Controller for a Field-Oriented Controlled BLDC Motor to Achieve the Desired Angular Velocity and Torque

H.R. Jayetileke*[1], W.R. de Mel[2], H.U.W. Ratnayake[3]

Submitted: 23/05/2019 Accepted : 18/09/2019

Abstract: Compared to traditional motor controlling techniques, modern AI controllers have many advantages. However, most of the developed FOC mechanisms are based on classical controlling techniques such as PID controllers, hybrid AI-classical controllers and model reference controllers. All these traditional controllers are based on sophisticated mathematical models (system transfer functions). These traditional controllers are unable to tune its system parameters by it-self to adapt according to the non-linear variations of actual speed and torque of the motor.

This paper discussed, a novel scheme of metaheuristic adaptive fuzzy logic-particle swarm optimization control mechanism to optimize the speed regulation of electric current space vector-controlled BLDC motor. Therefore, dynamic TSK-PSO-FLC was investigated. The dynamic behaviour of the proposed controller enables it to optimize its tuning parameters by it-self under non-linear load and speed varying conditions to track the desired angular speed and the torque trajectories.

This is a part of the designed and developed dynamic AI controller, for stability and traction control of an all-wheel-drive electric rover. Therefore, initially, the performance of the proposed controller has been tested on a simulation environment (MATLAB Simulink model) for one wheel. Finally, the identified dynamic parameters through the Simulink model (the sensored BLDC motor and the proposed AI controller) were utilized to test the performance of the developed TSK-PSO-FLC, while it is tracking a given desired speed trajectory of the BLDC motor (sensored, 3-ph and 250 W) in real-time operation.

Simulated test results are analyzed and compared with the observed test results through the developed hardware model in addition to the newly published research work. The angular speed of 2500 rpm within a 500 N m torque have been taken into consideration as a generalized condition. It was noticed that the percentage overshoot (*Mp%*), settling time (T_s) and the steady-state error (E_{ss}) is 0.501, 731.455 µs and 1.22 respectively. Therefore, compared to classical control based FOC mechanisms, the analyzed test results of the proposed control mechanism is showing that it has been optimized and enhanced the speed regulation performance of the BLDC motor significantly while increasing the frequency of the desired input trajectory up to 2 kHz.

Keywords: *Brushless direct current (BLDC) motor, Fuzzy logic (FL), Field-oriented control (FOC), Particle swarm optimization (PSO)*

1. Introduction

In industrial applications, 90% of motor drives have AC Induction Motors (IMs) because of simple operation and cost-effective driving mechanism due to non-use of Variable Frequency Drives (VFD) [1]. Compared to conventional brushed DC motors, IMs are more durable. However, compared to Permanent Magnet Synchronous Motors (PMSM), IMs are less efficient, and in long-time operations, energy wastages are significant [1]. PMSMs are the same as the AC IMs which has stator windings around the stator and with a Permanent Magnet (PM) rotor instead of using a wound rotor to generate a rotor magnetic field.

A PMSM could be utilized as a trapezoidal type BLDC motor when energizing only two phases at each time with six-steps electronically communication commutator system through Hall Effect sensors. Because of energizing only two phases at each period, it reduces the rotor resolution. To overcome this problem, in a PMSM the exact rotor position is measured and energized for all the three phases to produce a rotating magnetic field in the stator. Then the PMSM is known as a sinusoidal type BLDC motor. Rather than utilizing for industrial applications sinusoidal type BLDC motors are mostly used in the field of automobiles, because sinusoidal type BLDC motors have enhanced performance such as smooth torque and speed characteristics and low noises compared to trapezoidal type BLDC motors. However, according to the need of exact rotor position in sinusoidal type BLDC motors, high-resolution absolute encoders are utilized, and this increases the project cost and extra maintenance cost.

As a solution without measuring the rotor position, only measuring the current and voltage in 2-phases (because the remaining phase current could be calculated according to Kirchhoff's current law) the exact rotor position could be estimated more precisely and generate the required resultant magnetic force through this newly develop TSK-PSO-FL controller. In a PMSM, detection of the rotor position through the measured voltage and current in two phases and controlling the stator magnetic field through the 3-ph stator voltage and current which is known as electric current space FOC or Vector Controlled (VC). The advantage is in FOC mechanism, which enables it to generate a smooth resultant rotating magnetic force as expected according to the proposed TSK-PSO-FL controller output even under low-speed conditions and where the Direct Torque Control (DTC) mechanism which

[1] *Mechatronics Eng., The Open University of Sri Lanka, SRI LANKA*
ORCID ID: 0000-0001-5967-4198
[2] *Mechanical Eng., University of Sri Jayewardenepura, SRI LANKA*
ORCID ID: 0000-0002-4858-9630
[3] *Computer Eng., The Open University of Sri Lanka, SRI LANKA*
ORCID ID: 0000-0002-2178-9261
** Corresponding Author Email: hrjay@ou.ac.lk*

reduces performance. The other significant problem arrives in motor control applications because of the non-linearity varying load conditions and speed fluctuations (overshoots and undershoots) a long settling time takes place. Therefore, most of the research work has been published according to Artificial Intelligent (AI) and conventional methods during the past decades to optimize the speed regulation performance within a minimum settling time of brushed and brushless motors during the acceleration and deceleration.

2. Similar Research Work

N. Jayamary Sujatha and M. Saravanan have published their work based on combining FL with classical control systems according to closed-loop control strategies under load and no-load conditions [2]. Everson B. Siqueira et al. have proposed a new algorithm to utilize classical Proportional-Integral (PI) controller with enhanced performance for more robustness conditions of BLDC motors [3]. Mohd Tariq et al. have proposed and implemented an Antiwindup PI speed controller for a BLDC motor on a Digital Signal Processing (DSP) board. They can completely avoid the overshoot and to reduce the settling time up to 0.1 seconds at 100% load starting condition. Their experimental results have been presented for a step input response [4]. Adel A. El-samahy and Mohamed A. Shamseldin have designed and developed a DC motor tracking controller which is using self-tuning fuzzy Proportional-Integral-Derivative (PID) control and model reference adaptive control mechanisms, and their work was presented based on a MATLAB Simulink model [5]. In this proposed method, because of using classical control techniques and adaptive model-based techniques, the exact mathematical model needs to be derived through the governing equations. K. Premkumar and B.V. Manikandan paper discussed the designing and testing of a BLDC motor controller which was based on classical controlling techniques while tuning through a nature-inspired optimization algorithm such as the Bat Algorithm (BA) and where the BLDC motor has driven according to trapezoidal type BLDC motor driving techniques which reduces the performance during low speeds compared to FOC [6].

Their test results show that the minimum average computation time and the settling time around 4 minutes (248.7020 seconds) and 0.0205 seconds, respectively. Ahmed Rubaai and Paul Young have presented a “Hardware / Software implementation of fuzzy Artificial Neural Network (ANN) self-learning control methods for BLDC motor drives” [7]. In this proposed mechanism to generate the most appropriate fuzzy rule matrix, the heuristic capabilities of ANN have been utilized. The optimum performance has been achieved while training the ANN through an Extended Kalman Filter (EKF). However, as the author has mentioned the EKF mechanism is “computationally intense”. Thus, for high frequency desired input signal trajectories and for a long period of operation, more heat will generate on the processor which make a tendency to reduce the optimum performance of the controller. H.E.A. Ibrahim et al.’s paper describes the speed regulation of a BLDC motor through a PID controller and where the P, I and D gains have been optimized with PSO technique and Bacterial Foraging (BF) technique [8].

Compared to the BF technique, the PSO technique has improved the desired step response characteristics by minimizing the maximum overshoot, settling time and steady-state error by 0.5698 %, 0.0047 seconds and 0.0368 seconds, respectively. Reference [9] shows that A.S. El-Wakeel et al. had combined these BF and PSO techniques for optimal tuning of the PID controller of a PM-BLDC motor. The best-recorded settling time is 0.5 seconds under BF-PSO tuning criteria. Reference [10], [11], [12] and [13] shows other newly published similar research work, and some of these test results have been compared with the proposed controller as mentioned in Table 5.

As mentioned above, during the past few years researches work has made a substantial step forward in PM-BLDC motor controlling with AI or with combined AI and classical control methods compared to pure classical controlling methods. However, a comprehensive mechanism or algorithm is not available for modelling and analysis of TSK-PSO-FL controlled PM-BLDC motor using FOC techniques. Most of the stochastic search optimization techniques are static which utilize fixed tuning parameters such as the fixed population size, number of generations, crossover rate, mutation rate, acceleration constants and inertia weights. The proposed TSK-PSO-FL controller is an optimized dynamic controller in real-time, which is always adapt its parameters and the Membership Function (MF) gains between the consequent and antecedent while generating the optimum rule matrix. In this paper, modelling the PM-BLDC motor according to FOC techniques, the complete MATLAB Simulink simulation and

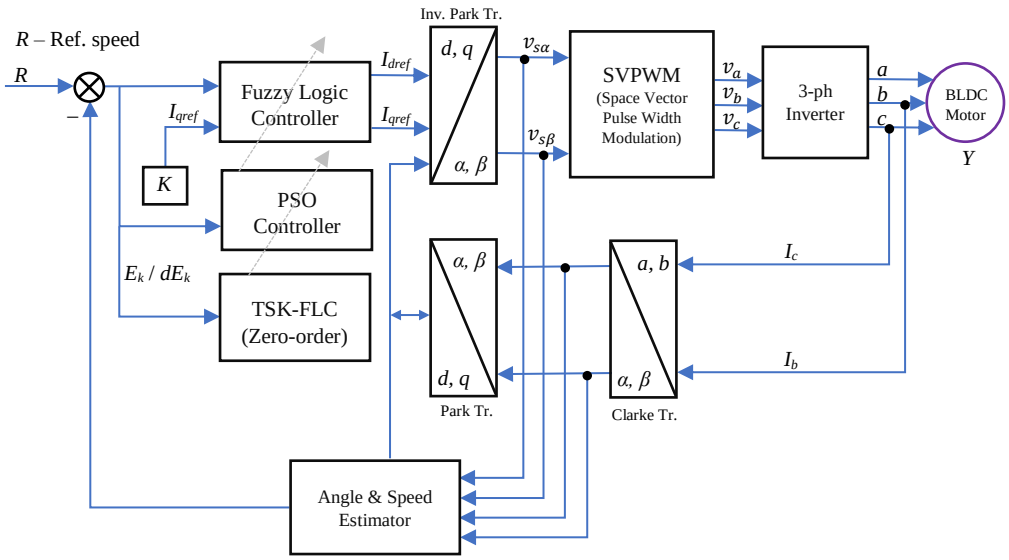

Fig. 1. Overall system block diagram representation

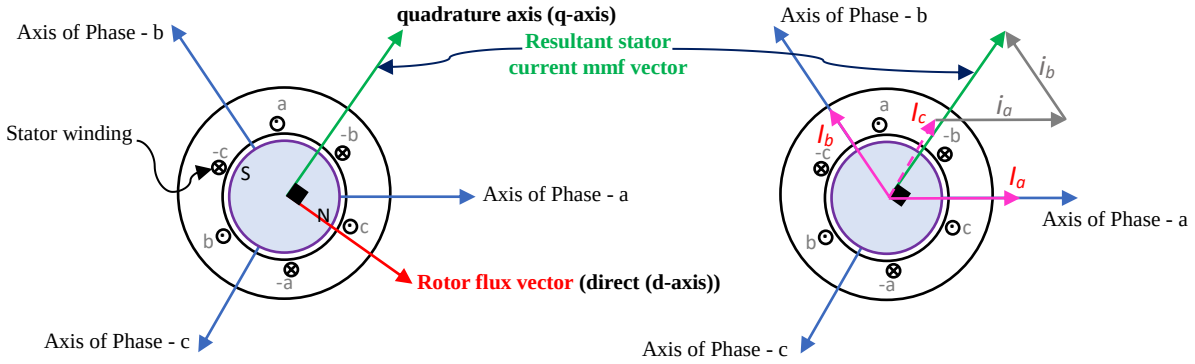

Fig. 2. Stator current *mmf* vector with respect to the rotor flux vector

the experimental test results are presented and analyzed to validate the performance compared to past researcher's work.

Rest of this paper is organized as follows. Section 3 has described the overall system mechanism of the TSK-PSO-FLC and the PM-BLDC motor, according to FOC and closed-loop control strategies. Section 4 discusses the mathematical model and the detail Simulink model of the PM-BLDC motor while taking into account the FOC concepts. Section 5 explains the TSK-PSO-FLC according to AI concepts. The simulation test results are presented, analyzed and compared with other similar research work in detail in Section 6. Finally, Section 7 concludes this paper with the final achievements and future developments.

3. Overall System Mechanism

The proposed TSK-PSO-FL controller, as shown in Fig. 1, is designed and constructed according to the closed-loop control strategies which are able to rapidly reduce the error (*E*) and the rate of changing error (*dE*) with the acquisition of the desired angular speed and the actual angular speed information of the PM-BLDC motor. The *E* and *dE* compute for every instant iteration or sample (*k*) through the TSK-PSO-FL controller according to (1) and (2), where *R* and *Y* are the reference signal or the desired output and the actual output respectively. In the simulation model, the main Mamdani type FL controller consists of pre-defined 21 Linguistic Variables (LVs), 21 MFs and 49 Fuzzy Rules (FR) (7^2).

$$E_k = \left(R_k - Y_k\right) \tag{1}$$

$$dE_k = E_k - E_{k-1} \tag{2}$$

In addition to these static MFs and FRs, dynamic fuzzy MFs and FRs take place in real-time which are continuously tuning through the PSO controller for every sample instant "*k*" and where the combined FL-PSO controller algorithm is running in a MATLAB ".m" file. During the real-time simulation process, the "Interrupted MATLAB Fcn" block, is interrupting the simulation process and feeding the newly updated parameters to the PM-BLDC motor Simulink model very quickly and precisely. While interacting the Simulink model with the FL-PSO controller (.m file) through the aforementioned "Interrupted MATLAB Fcn" block, another separately dedicated zero-order Takagi-Sugeno-Kang (TSK) FL controller (TSK-FLC), tunes the parameters of the PSO controller. As shown in Fig. 1 according to the closed-loop control strategies, the inner closed-loop path always regulates the amount of current flowing in the BLDC motor to achieve the desired torque. In the outer closed-loop path, the angular-speed estimator will generate the error signal (compering with the commanded signal) and feed into the proposed controller. In this current mode control mechanism, the following steps have been taken into account when designing and constructing the Simulink model. Measure the amount of current already flowing in the motor, as shown in Fig. 1. Compare the measured current with the desired current and the amount of error and the rate of changing error feed into the proposed controller, through the controller, adapt and amplify the error signal to generate the correction voltage (If the current is high decrease the voltage and if the current is low increase the voltage). After that modulate the correction voltage onto the motor as sown in Fig. 1, through the Clarke transformation, Park transformation and inverse Park transformation process. All these aforementioned steps are repeated for every sample instance "*k*".

In a PM-BLDC motor when the stator current *mmf* vector is right on top of the rotor flux vector (direct or the d-axis) then the torque is zero. Therefore, to achieve the maximum torque in this electric current space vector FOC mechanism, always the stator current *mmf* vector should be right angle (90^0 degrees) to the rotating rotor flux vector (on the quadrature or q-axis) as shown in Fig. 2. The torque produced by the PM-BLDC motor is given by (3); where; T_e: electrical torque, P: number of poles, ψ_r: rotor flux, I_{ds} & I_{qs}: stator current vector and L_d & L_q d-axis and q-axis stator self-inductance.

$$T_e = \frac{3}{2}\frac{P}{2}\left[\psi_r I_{qs} + \left(L_d - L_q\right) I_{qs} I_{ds}\right] \tag{3}$$

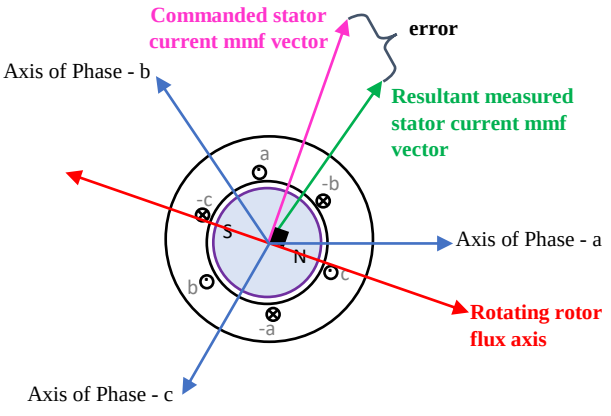

Fig. 3. The commanded stator current vector respect to the rotor flux vector

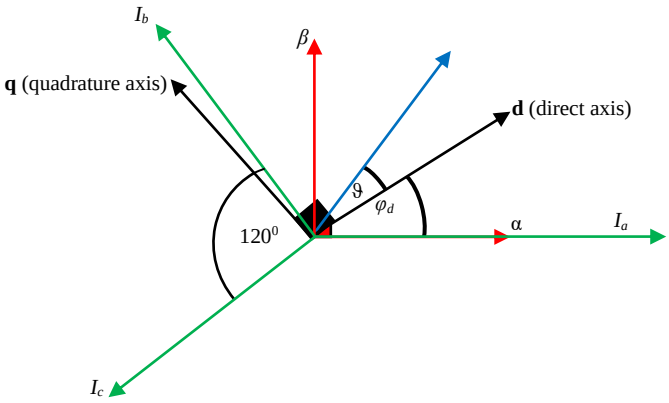

Fig. 4. The stationary 3-axis reference frame (*a-b-c*), stationary 2-axis frame (α-β) and the rotating reference frame (*d-q*)

According to (3), to control the torque of the motor then only the magnitude of the stator current vector will be regulated through the proposed controller instead of varying the angle of the stator current vector. After measuring the stator current vector, compared the measured current vector with the desired current vector and then generated the error and the rate of changing error signals for the proposed controller. The angle and the magnitude of the desired stator current vector depend on the angle of the rotor flux vector and the required amount of torque, respectively. As shown in Fig. 3, if there is an error between the measured stator current vector and the commanded stator current vector, then this was corrected through the magnitude and the angle of the stator current vector by regulating the stator current I_a, I_b and I_c through the proposed controller.

As shown in Fig. 3, the stator current vector magnitude and the angle could be represented with a two-axis coordinate system. That means the 3-ph PM-BLDC motor could simplify into a 2-ph motor. The stator current vector was measured with respect to the stationary stator reference frame. However, the angular error needs to calculate with respect to the rotating rotor reference frame. Therefore, the stator current vector which was measured with respect to the stationary reference frame (*a-b-c*) need to be converted into a two-axis stationary reference frame (α-β frame) and then converting it again to a rotating reference frame (*d-q* frame) to calculate the angular error between the stator current vector and rotor flux vector and finally converting it back into the stationary reference frame (*a-b-c*) as shown in Fig. 4.

4. Mathematically based, Simulink Model of The PM-BLDC Motor

In this research, the main goal is to test the proposed control mechanism instead of modelling an exact PM-BLDC motor using optimum parameters. Therefore, the cogging torque between the PMs and stator teeth, reluctance torque (due to position-independent inductance), core losses, magnetic saturation and temperature effects to the electrical parameters have been neglected. Therefore, the simplified model governing equations of the PM-BLDC motor could be expressed as (4), (5), (6) and (7).

$$V_{qs} = \left(R_s + \frac{d}{dt} L_{qs} \right) I_{qs} + \omega_e L_{ds} I_{ds} + \omega_e \psi_r \tag{4}$$

$$V_{ds} = \left(R_s + \frac{d}{dt} L_{ds} \right) I_{ds} - \omega_e L_{qs} I_{qs} \tag{5}$$

$$\omega_e = \frac{P}{2} \omega_r \tag{6}$$

$$J \frac{d}{dt} \omega_r = T_e - T_L - B\omega_r \tag{7}$$

where; V_{ds} & V_{qs}: *dq*- axis components of stator phase voltage (V), I_{ds} & I_{qs}: *dq*-axis components of stator phase current (A) R_s: stator resistance (Ω), L_{ds} & L_{qs}: *d* & *q* axis stator self-inductance (H), ω_e: electrical angular speed (rad/s), ω_r: angular speed of the rotor (rad/s), ψ_r: rotor magnetic flux (Wb), *P*: number of poles, *J*: moment of load inertia (kg m^2), T_e & T_L: electrical and load torque (N m) and *B*: viscous coefficient of the load (kg m^2/s).

According to (4), (5), (6) and (7) in this proposed control mechanism regulating the quadrature current has been taken into account through the aforementioned frame transformations. Regulating the electric current respect to the *d-q* frame (rotating rotor reference frame) and which is flowing into the PM-BLDC motor has been achieved through regulating the voltage respect to the stationary reference frame (*a-b-c* frame). For this process following steps have been taken into account.

- The measured I_a, I_b and I_c respect to the stationary reference frame (*a-b-c* frame) converted into a 2-axis stationary reference frame (α-β frame) according to (8), (9) (forward Clark transformation);

$$I_\alpha = \frac{3}{2} I_a \tag{8}$$

$$I_\beta = \frac{\sqrt{3}}{2} I_b - \frac{\sqrt{3}}{2} I_c \tag{9}$$

- The calculated electric current respect to the α-β frame converted into a 2-axis rotating rotor reference frame (*d-q* frame) according to (10) and (11) to obtain I_{ds} and I_{qs}. (forward Park transformation).

$$I_{ds} = I_\alpha \cos\varphi_d + I_\beta \sin\varphi_d \tag{10}$$

$$I_{qs} = -I_\alpha \sin\varphi_d + I_\beta \cos\varphi_d \tag{11}$$

- According to the E_k & dE_k the commanded new I_{ds} and I_{qs} calculated and obtained the new V_{ds} and V_{qs} in the same *d-q* frame according to (4) and (5).

- The new V_{ds} & V_{qs} have been converted into the α-β frame to obtained V_α & V_β as in (12) & (13).

$$V_\alpha = V_{ds} \cos\varphi_d - V_{qd} \sin\varphi_d \tag{12}$$

$$V_\beta = V_{ds} \sin\varphi_d + V_{qd} \cos\varphi_d \tag{13}$$

- Finally, the V_α and V_β converted into the *a-b-c* stationary reference to obtain the new commanded voltage V_a, V_b and V_c to regulate the speed and torque of the PM-BLDC motor (reverse Clark transformation) as shown in (14), (15), & (16);

$$V_a = \frac{2}{3} V_\alpha \tag{14}$$

$$V_b = -\frac{1}{3} V_\alpha + \frac{1}{\sqrt{3}} V_\beta \tag{15}$$

$$V_c = -\frac{1}{3}V_\alpha - \frac{1}{\sqrt{3}}V_\beta \tag{16}$$

As shown in Fig. A.1 and Fig. A.2 mentioned in Appendix - A, when modelling the PM-BLDCM according to (3), (4), (5), (6) and (7), it was separated into the main three parts (a, b and c) such as PM-BLDCM rotor reference frame-block, electrical torque block and the PM-BLDCM dynamic model block (include the electrical and mechanical torque behaviour, angular velocity, inertia and the viscous damping effects). The subsystems of these main three blocks have expanded, and the inputs and outputs of each block have named according to the main governing equations of the PM-BLDC motor.

5. TSK-PSO Fuzzy Logic Controller

5.1 Dynamic PSO Mechanism (DPSOM)

The proposed TSK-PSO-FL controller is a dynamic-metaheuristic optimization mechanism which was based on biologically inspired (birds flock and fish school in search of food) PSO and FL techniques. When controlling a PM-BLDC motor, the behaviour is highly non-linear and robust due to the non-linearly varying angular velocity and mechanical torque. Therefore, the error and the rate of changing error is highly non-linear, discontinuous and non-differentiable due to the aforementioned factors that cause the objective function of the PSO mechanism to become non-linear and the inputs and output of the FLC towards non-precise. Reference [14] shows that PSO technique is highly efficient and fast convergence compared to GA because in GA it is not taking into account the past emergent performance (GA is a serial strategy, and PSO is a parallel strategy). In this proposed controller the main goal of the dynamic PSO mechanism is to identify the set of optimum parameters which was utilized to tuned the Mamdani type FLC while minimizing the objective function (a function of E_k and the dE_k). These optimum parameters are the final solution of the PSO controller which was generated while taking into account the personal-best (P_{Best}) of each particle (feasible solutions) until reaching the global-best (G_{Best}) or the social best solution in the search space. These parameters need to be quickly re-optimized because of the dynamic behaviour of the PM-BLDC motor. As shown in Fig. 5 the updated positions of the particles are determined by taking into account the updated velocity.

In the hyperspace, if the position of the particle "*i*" is denoted by x_i (t) at a discrete-time t then the updated position x_i ($t+1$) and the updated velocity v_i ($t+1$) is determined according to (17), (18) and [15],

$$x_i(t+1) = x_i(t) + v_i(t+1) \tag{17}$$

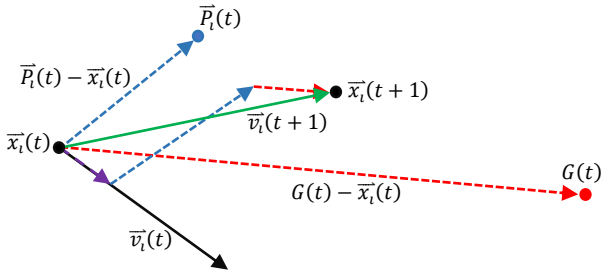

Fig. 5. Geometric representation of the PSO model

$$v_i(t+1) = \omega.v_i(t) + r_1 a_1\left(P_{i_{Best}}(t) - x_i(t)\right) + r_2 a_2\left(G_{Best}(t) - x_i(t)\right) \tag{18}$$

where; ω : inertia weight, $v_i(t)$: velocity at a time step t, r_1, r_2: randomly generated and uniformly distributed numbers, $0 \le r_1 \le 1$, $0 \le r_2 \le 1$, a_1, a_2: acceleration coefficients, $P_{i_{Best}}$: personal best and G_{Best} : global best.

As described in Section 5.2, eighteen number of variables are utilized to tune the Mamdani type FLC (the main controller). Therefore, eighteen number of dimensions are taken into account in the hyperspace when designing the proposed dynamic PSO mechanism. In a traditional PSO mechanism, all the candidate solutions or particles are unattainable to convergence to an equilibrium position due to the rapid changes in the amplitude and the frequency of the desired input trajectory (the dynamic behaviour). To overcome this problem, in the proposed TSK-PSO-FL controller, the parameters of the dynamic PSO mechanism was tuned in real-time through a separately dedicated TSK-FLC as described in Section 3. Through this TSK-FLC, for every iteration or discrete sample re-initialized the particle positions (solutions) by optimizing the population size ($nPop$), inertia weights (ω_{max} and ω_{min}), acceleration coefficients (a_1 and a_2) and charged the PSO by adding a dynamic acceleration (a_f) into the standard equation (18). Finally, this eighteen-dimensional proposed dynamic PSO mechanism could be expressed as shown in (19) and (20),

$$x_{ij}(t+1) = x_{ij}(t) + v_{ij}(t+1) \tag{19}$$

$$v_{ij}(t+1) = \omega.v_{ij}(t) + r_1 a_1\left(P_{ij_{Best}}(t) - x_{ij}(t)\right) + r_2 a_2\left(G_{jBest}(t) - x_{ij}(t)\right) + a_{ij}(t) \tag{20}$$

where: $a_i(t) = \frac{1}{K}\left[\left(\sum_{p=1, i\neq p}^{nPop} a_{ip}\right) \Big/ (nPop)\right]$, $K \in \mathbb{R}$, $nPop$: population size, $j \in \mathbb{Z}^+$, $1 \le j \le 18$, $r_1 a_1\left(P_{ij_{Best}}(t) - x_{ij}(t)\right)$: Cognitive component and $r_2 a_2\left(G_{jBest}(t) - x_{ij}(t)\right)$: Social component. The cognitive component and the social component have taken into account its previous best solution and the global best solution, respectively. In this mathematical model for the proposed dynamic mechanism, the inertia weight has been computed according to (21) and continuously optimized through the TSK-FLC.

$$\omega = \omega_{\max} - \left(\frac{\omega_{\max} - \omega_{\min}}{MaxIter}\right) * Iter \tag{21}$$

where: ω_{max}, ω_{min}: maximum and minimum inertia weights assigned in the TSK-FLC, *MaxIter:* Maximum no. of iterations and *Iter*: current iteration.

To combined this PSO mechanism and the main Mamdani type FLC, an objective function Ob_f has utilized as the input to the PSO mechanism which is a function of the E_k and the dE_k as shown in Fig. 1. In this dynamic environment for a rapid convergence and to enhance the performance of the PSO mechanism an objective function index I_{Ob_f} has been taken into account while applying a

penalty on each constraint violation. The I_{Ob_f} computes according to (22) and (23),

$$Ob_f = RMSE = \sqrt{\frac{1}{N}\sum_{k=1}^{N}\left(e_k(t)\right)^2} \tag{22}$$

$$I_{Ob_f} = Ob_f + \left(\sum_{k=1}^{N} e_k\right) * \text{penalty} \tag{23}$$

where: $\sqrt{\frac{1}{N}\sum_{k=1}^{N}\left(e_k(t)\right)^2}$: root mean square error

5.2 TSK-FLC (Takagi-Sugeno-Kang Fuzzy Logic Controller)

The output level "Z" of the TSK-FLC could be expressed as (24),

$$Z_k = a\left(E_k\right) + b\left(dE_k\right) + c \tag{24}$$

The constructed TSK-FLC contains 16 number of FRs and where the; a, b and c are constants and ($a=b=0$). That means the output level is always a constant and not a linear function. When the firing strength of a particular FR is w_k for a k^{th} sample, and when each FR is interacting with a "AND" operator then the firing strength could be defined as (25),

$$w_k = Andmethod\left(MF_i(E), MF_i(dE)\right) \tag{25}$$

where; $MF_i(E)$ and $MF_i(dE)$ are input MFs for the i^{th} linguistic variable ($i \in \mathbb{Z}^+$ and $1 \le i \le 7$). In the TSK-FL controller for all the 16 FRs, the weighted average final output has computed as (26),

$$Output_{(\text{TSK}-\text{FL})} = \frac{\sum_{i=1}^{16} w_i Z_i}{\sum_{i=1}^{16} w_i} \tag{26}$$

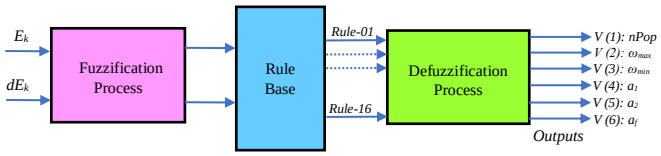

Fig. 6. Block diagram of the TSK-FLC

Table 1. Governing fuzzy rules of the proposed TSK-FL controller

No.	Inputs		Outputs					
	E_k	dE_k	nPop	ω_{max}	ω_{min}	a_1	a_2	a_f
01	PVS	PVS	PS	PM	PM	PM	PM	None
02	PS	PVS	PS	PM	PM	PM	PM	None
03	PM	PVS	PM	PB	PM	PM	PM	None
04	PB	PVS	PB	PB	PB	PB	PB	PS
05	PVS	PS	PS	PM	PM	PS	PS	None
06	PS	PS	PM	PM	PM	PM	PM	None
07	PM	PS	PM	PB	PB	PM	PM	None
08	PB	PS	PB	PB	PB	PB	PB	PS
09	PVS	PM	PM	PM	PM	PM	PM	None
10	PS	PM	PM	PB	PM	PM	PM	None
11	PM	PM	PM	PB	PB	PM	PM	None
12	PB	PM	PB	PB	PB	PB	PB	PS
13	PVS	PB	PM	PM	PM	PM	PM	None
14	PS	PB	PM	PB	PB	PM	PM	None
15	PM	PB	PB	PB	PB	PM	PM	None
16	PB	PB	PB	PB	PB	PB	PB	PS

The output of the TSK-FLC determined according to (24), (25), and (26). As shown in Fig. 6, the six output parameters of the TSK-FLC which are inputs to the dynamic PSO mechanism and tuned in real-time according to the rapid changes of the E_k and dE_k.

Figure 7 shows the membership functions, boundaries of each fuzzy set (MF) and where the "PVS", "PS", "PM" and "PB" represents the Positive very small, Positive small, Positive medium and Positive big LVs respectively. Table 1 shows, the main governing FRs of the TSK-FL controller. In this TSK-FL controller, the outputs are always constants (not a linear function). According to each output, the practically verified linguistic values of the LVs are as shown in Table 2.

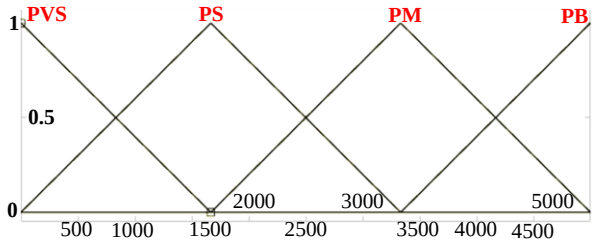

Fig. 7. Membership functions of E_k and dE_k

Table 2. Assigned linguistic values for the linguistic variables of the TSK-FL controller

	TSK-FL controller Outputs					
Linguistic Variables	*nPop*	ω_{max}	ω_{min}	a_1	a_2	a_f
PVS	5	0.800	0.100	0.975	0.975	None
PS	10	0.825	0.300	0.985	0.985	0.009
PM	15	0.875	0.400	0.995	0.995	None
PB	20	0.900	0.500	1.000	1.000	None

5.3 Mamdani type FLC (the main FLC)

As shown in Fig. 8 and Fig. 9, while optimizing the Gaussian curve MFs through the gain factors (optimized solutions of the dynamic PSO mechanism such as G_{jBest}) the proposed Mamdani type FL control mechanism is dynamically optimized through the dynamic fuzzification, de-fuzzification and with static and dynamic FRs. As shown in Fig. 8 and (27) symmetric Gaussian curve MFs have been taken into account for the fuzzification and de-fuzzification process.

$$f\left(x;\sigma,c\right) = \exp\left(-\frac{1}{2}\left(\frac{x-c}{\sigma}\right)^2\right) \tag{27}$$

where: c is the peak value of the center and σ is the width of the curve.

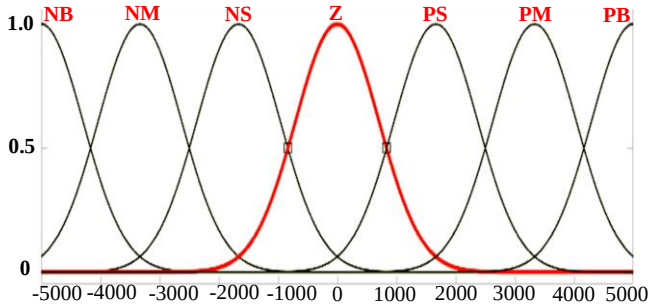

Fig. 8. Membership functions of Mamdani FLC (E_k, dE_k *and* U_k)

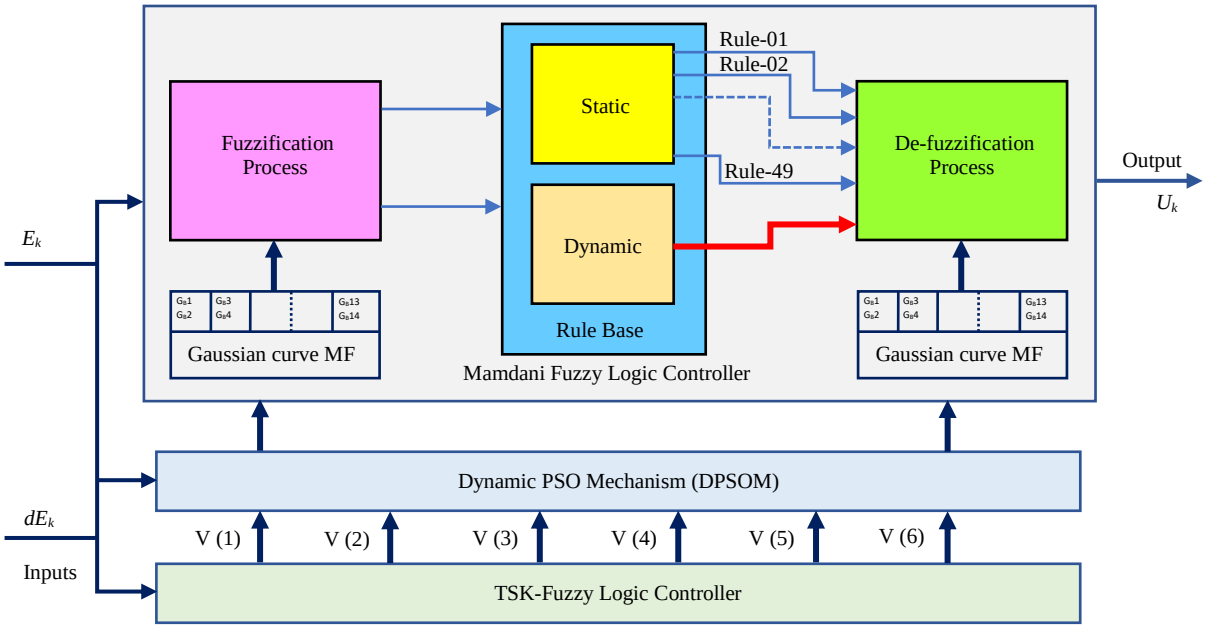

Fig. 9. The main dynamic FL controller

The dynamic gains of the Mamdani FLC, have been computed for the peak value c and for the standard deviation σ as (28) and (29).

$$gain_{c_i} = \pm\frac{1}{\lambda}\times\left(G_{jBest}\times 707\right) \tag{28}$$

$$gain_{\sigma_i} = \pm\frac{1}{\lambda}\times\left(G_{jBest}\times 5000\right) \tag{29}$$

where: $c_i \in (2Z^+ + 1), 1 \le c_i \le 13, \sigma_i \in 2Z^+, 2 \le \sigma_i \le 14$ and $\lambda_1, \lambda_2 \in \Re$

After computing the gain values for 14 dimensions which belong for the MFs the optimized peak value "c" and the standard deviation "σ" was calculated for each MF as shown in Table 3.
During the real-time optimization process the global solution of the PSO mechanism (eighteen dimensions for the solution) has been limited through the lower boundary (L_{Bj}) and the upper boundary (U_{Bj}) limits, 0 to 7 respectively. Reference [16] shows that, the utilized static FRs for this proposed Mamdani FLC (M-FLC) as shown in Fig. 9. Out of eighteen dimensions the three consequent dimensions solutions (solution of the global minimum of the dynamic PSO mechanism) before the final dimension are utilized to optimize the dynamic FRs of the M-FLC.
As shown in Fig. 8, number of seven LVs are utilized for this M-FLC, and the corresponding global solution values of each dimensions are as **"*NB = 1*"**, **"*NM = 2*"**, **"*NS = 3*"**, **"*Z = 4*"**, **"*PS = 5*"**, **"*PM = 6*"** and **"*PB = 7*"**.

Table 3. The optimized parameters of the symmetric Gaussian curve membership functions

Membership function	*c (optimized peak value)*	*σ (optimized standard deviation)*
NB	$c_1 = -5000 \pm gain_1$	$\sigma_2 = 707 \pm gain_2$
NM	$c_3 = -3333 \pm gain_3$	$\sigma_4 = 707 \pm gain_4$
NS	$c_5 = -1667 \pm gain_5$	$\sigma_6 = 707 \pm gain_6$
Z	$c_7 = 0 \pm gain_7$	$\sigma_8 = 707 \pm gain_8$
PS	$c_9 = 1667 \pm gain_9$	$\sigma_{10} = 707 \pm gain_{10}$
PM	$c_{11} = 3333 \pm gain_{11}$	$\sigma_{12} = 707 \pm gain_{12}$
PB	$c_{13} = 5000 \pm gain_{13}$	$\sigma_{14} = 707 \pm gain_{14}$

However, during the real-time optimization process always the global solution values (values of the consequent three dimensions before the final dimension) are not equal to these corresponding values.

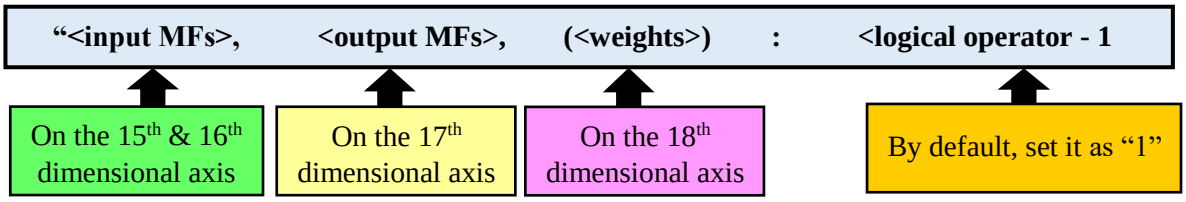

Fig. 10. The dynamic indexed rules format of the M-FLC

Therefore, out of these eighteen number of dimensions, the 15th, 16th and 17th dimension solutions of the dynamic PSO mechanism was rounded and assigned for the most suitable LV. In this M-FLC, the dynamic indexed rules format is as shown in Fig. 10.
For example, in real-time operation, if a dynamic FR was generated by the PSO-MFLC, and then the particular dynamic FR could be expressed as;

Generated dynamic fuzzy rule: **"2 5, 7 (0.75): 1"**

Meaning of this rule: **"IF Error = NM AND dError = PS THEN Speed = PB"**
(Because: "NM = 2", "PS = 5" and "PB = 7").
(the rule weight is "0.75"and the operator between the antecedents is "AND")

6. Analysis of The Simulation Test Results

As shown in Fig. 11 and Fig. 12, at a constant speed for varying high torque conditions (up to 2 kNm), at a constant torque for varying low-speed conditions (500 rpm) and for a square edge trajectory the proposed control mechanism is highly adaptive and stable. As shown in Fig. 13 and Table 4, the 1st loading condition (500 N m) performance parameters are good enough to compare with similar research work. Where these parameters are *Mp%*, T_s and E_{ss} are 0.501, 731.455µs and 1.22 respectively. The compared, similar research work performance parameter values are shown in the 5th column of Table 5. The 6th column test results show that the proposed dynamic controller has been significantly reduced the *Mp%*, T_s, and the E_{ss}.
Reference [17] shows, different trajectories are also utilized to test the performance of these type of controllers. Therefore, as the worst situation, a square type trajectory was utilized, and the stable frequency range of the proposed controller is up to 2 kH_z. Figure A.1 shows the overall Simulink model of the proposed controller and where the PM-BLDC motor has model according to FOC mechanism. Figure A.2 shows the main three Simulink blocks, which were model according to the governing equations described in Section 4. Figure A.3 to Fig. A.11 shows all the extracted blocks of the modelled PM-BLDC motor. Figure B.1 and Fig B.2 shows the stator current variation respect to the stationary (*a*-*b*-*c*) reference frame and the stator current variation respect to the 2-D stationary reference frame (α-β frame) when driving the PM-BLDC motor in real-time through the proposed controller respectively.
In addition to these simulation test results, the proposed AI control algorithm was tested on the developed hardware setup. In real-time operation, the proposed AI (TSK-PSO-FLC) controller is running on an Industrial Mobile Computer (IMC) according to the closed-loop control strategies. The desired input trajectory or the throttle signal for the PM-BLDC motor was transmitted to the motor drivers wirelessly, based on the IEEE 802.15.04 protocol through the forward path. As shown in Fig. C.1 to compute the E_k and the dE_k according to (1) and (2) a Hall-Effect sensor was utilized with PMs. The computed E_k and the dE_k of the motor rpm were again transmitted back to the IMC through the feedback path based on the protocol, as mentioned earlier.
Compared to combined classical-AI controllers [18] and AI controllers with static tuning parameters [19], the proposed TSK-PSO-FLC is a dynamic controller (where it could tune its parameters by it-self according to the E_k and dE_k). Moreover, compared to traditional DC motor driving techniques [20] the FOC mechanism could deliver the exact resultant magnetic force amount to the PM-BLDC motor (the generated electric torque "T_e") which was decided through the proposed dynamic AI controller.
Therefore, in addition to the simulation test results, the observed test results through the implemented hardware setup show that by combining the proposed dynamic AI control mechanism with the FOC mechanism have been significantly enhanced the performance of the PM-BLDC motor.

7. Conclusion

In this paper, a dynamic, TSK-PSO-FL controller was implemented which was based on PSO and FLC techniques for the FOC mechanism, in order to optimize the speed regulation of a PM-BLDC motor under sudden non-linear load changes during its fast acceleration and deceleration. The control parameters of the main M-FLC are not static, which are continuously updating and adapting according to the E_k and dE_k. These parameters are optimized through a PSO mechanism with a dynamic objective function and where the PSO parameters are also dynamically optimized through a TSK-FLC. According to the observed test results as a generalized condition the 1st loading condition in Table 4 shows that the proposed AI controller is highly stable and robust under non-linear varying speed-torque conditions because the overshoot is negligible and the T_s and E_{ss} are 731.455 µs and 1.22, respectively. Moreover, Fig. 11 shows that under very low speed and torque conditions, the system is highly stable. Figure C.4 shows that (the observed test results wirelessly based on the IEEE 802.15.04 protocol) the developed TSK-PSO-FLC is highly robust and stable because the deviations between the desired speed trajectory and the actual speed trajectory are negligible.

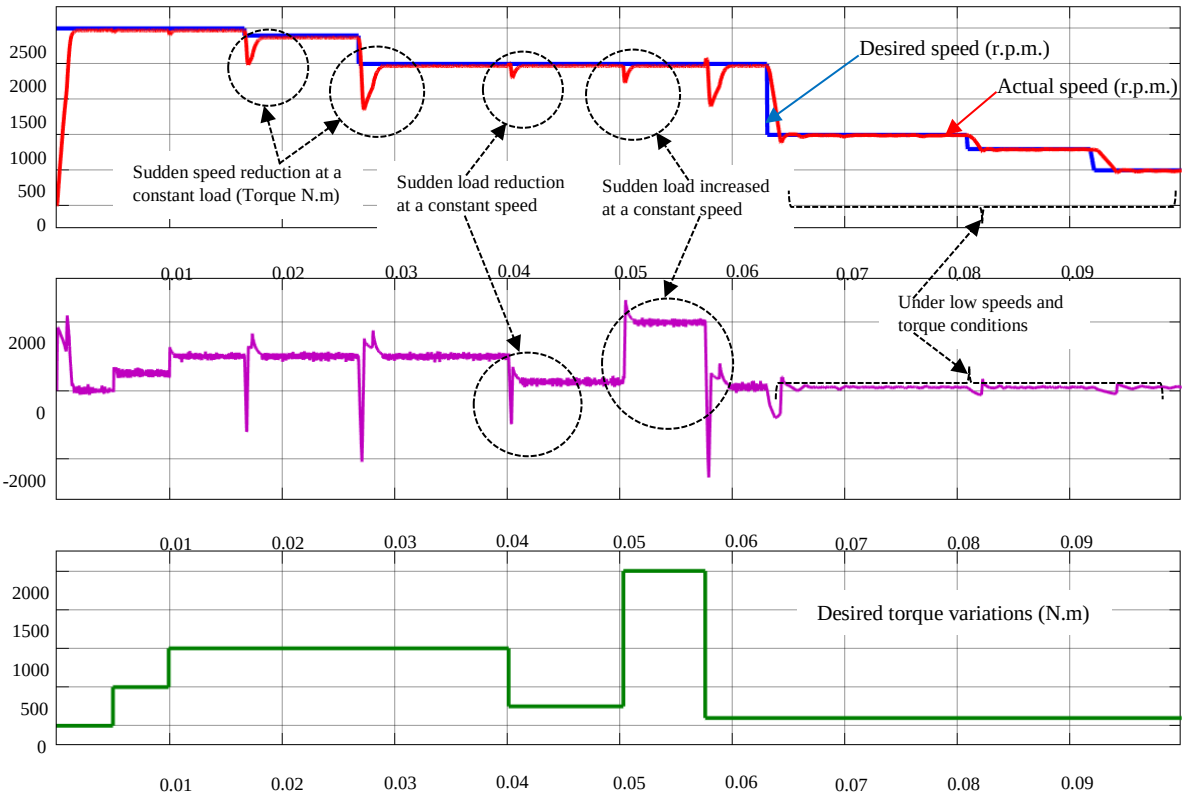

Fig. 11. Proposed TSK-PSO-FLC response for instant of sudden changes of desired speed and load

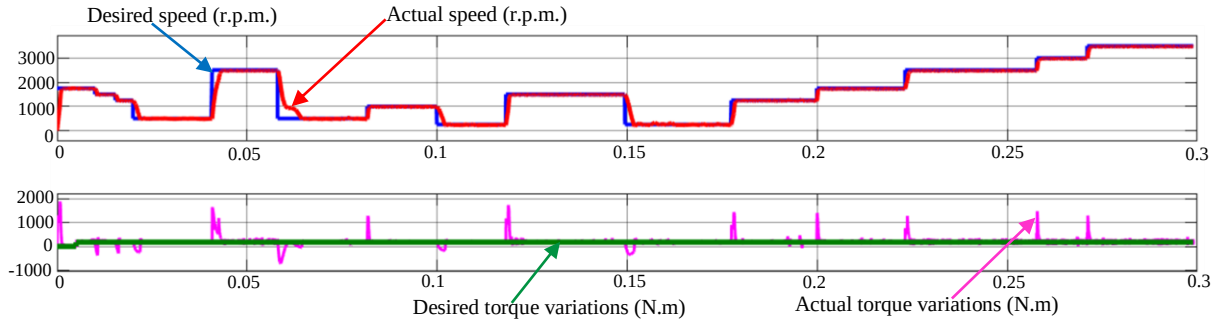

Fig. 12. The TSK-PSO-FL controller response for a Square input at a constant torque

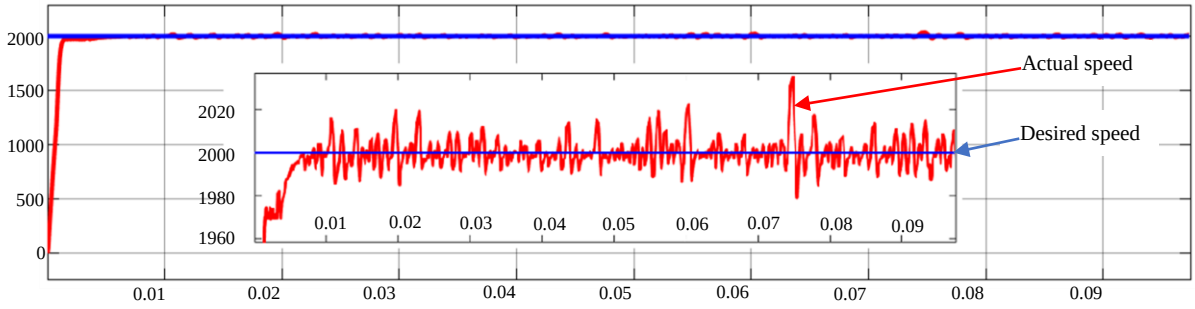

Fig. 13. The TSK-PSO-FL controller response for a Step input with loading conditions

Table 4. The proposed controller response during loading and non-loading conditions

r.p.m.	*Preshoot %*	*Overshoot M_p%*	*Undershoot %*	*Settling Time (T_s) (µs)*	*Rise Time (µs)*	*Steady state error (E_{ss})*	*Slew rate/µs*
1st Loading condition – 500 N m							
2000	0.510	0.834	1.365	577.459	876.123	1.20	1.786
2500	0.505	0.501	1.957	731.455	988.292	1.22	1.987
2nd Loading condition – 1000 N m							
r.p.m.	*Preshoot %*	*Overshoot M_p%*	*Undershoot %*	*Settling Time (T_s) (ms)*	*Rise Time (µs)*	*Steady state error (E_{ss})*	*Slew rate/µs*
2000	0.510	1.021	1.832	4.661	874.063	1.25	1.787
3000	0.505	0.505	2.798	4.524	1853.0	1.35	1.271
3rd Loading condition – 1500 N m							
r.p.m.	*Preshoot %*	*Overshoot M_p%*	*Undershoot %*	*Settling Time (T_s) (ms)*	*Rise Time (µs)*	*Steady state error (E_{ss})*	*Slew rate/µs*
2000	0.510	1.021	1.832	4.895	874.063	1.28	1.787
3000	0.505	0.505	12.964	8.498	1853.0	1.46	1.271

Table 5. Comparison of the proposed controller response (as shown in Table 4) with similar research work

Reference	*Speed (r.p.m.)*	*Load (N m)*	*Control mechanism*	*Test results of the Performance parameters*			*Performance parameters reduced percentage of the proposed controller*		
				T_s (Sec)	*M_p %*	*E_{ss}*	*T_s*	*M_p*	*E_{ss}*
[2]	2000	0.3	PI Controller	0.1550	10.60	1.00	212	21	0.83
			Fuzzy Logic Controller	0.1150	7.00	0.95	157	14	0.79
			Hybrid Fuzzy-PID	0.1200	None	0.90	164	-	0.75
[21]	1222	29.2	PID-PSO	0.0030	None	None	4	-	-
			Fuzzy-PSO	0.0100	None	None	14	-	-
[8]	100	4.0	PSO-(PID)	0.0047	0.5698	0.037	6	1.14	0.03
			BF-(PID)	0.0053	None	0.056	7	-	0.05
[9]	2000	1.2	PID-BF-PSO with ITAE and WGAM criteria	0.4850	3.4241	0.019	663	7	0.016
[22]	15	-	PID-(Ziegler-Nichols)	6.2220	29.2329	0.5	8506	58	0.417
			PID-(Cohen-Coon)	12.6787	36.8658	0.5	17,333	74	0.417
[23]	2400	-	PID-(Ziegler-Nichols)	0.2300	38.0	0.142	314	76	0.118
			PID-PSO	0.0630	0.0	0.0023	86	-	0.0019
[13]	1*	1*	APSO	0.3	0.0161	None	410	-	-
			PSO	0.7790	0.1092	None	1065	-	-
			GA	0.5500	0.0030	None	752	-	-
			PID-PSO-ZN	0.3054	None	None	418	-	-
[4]	1500	1.9	PI	0.6	1.7	-	820	3.39	-
			Antiwindup PI	0.1	None	-	137	-	-

* - Unit step response

Appendix – A

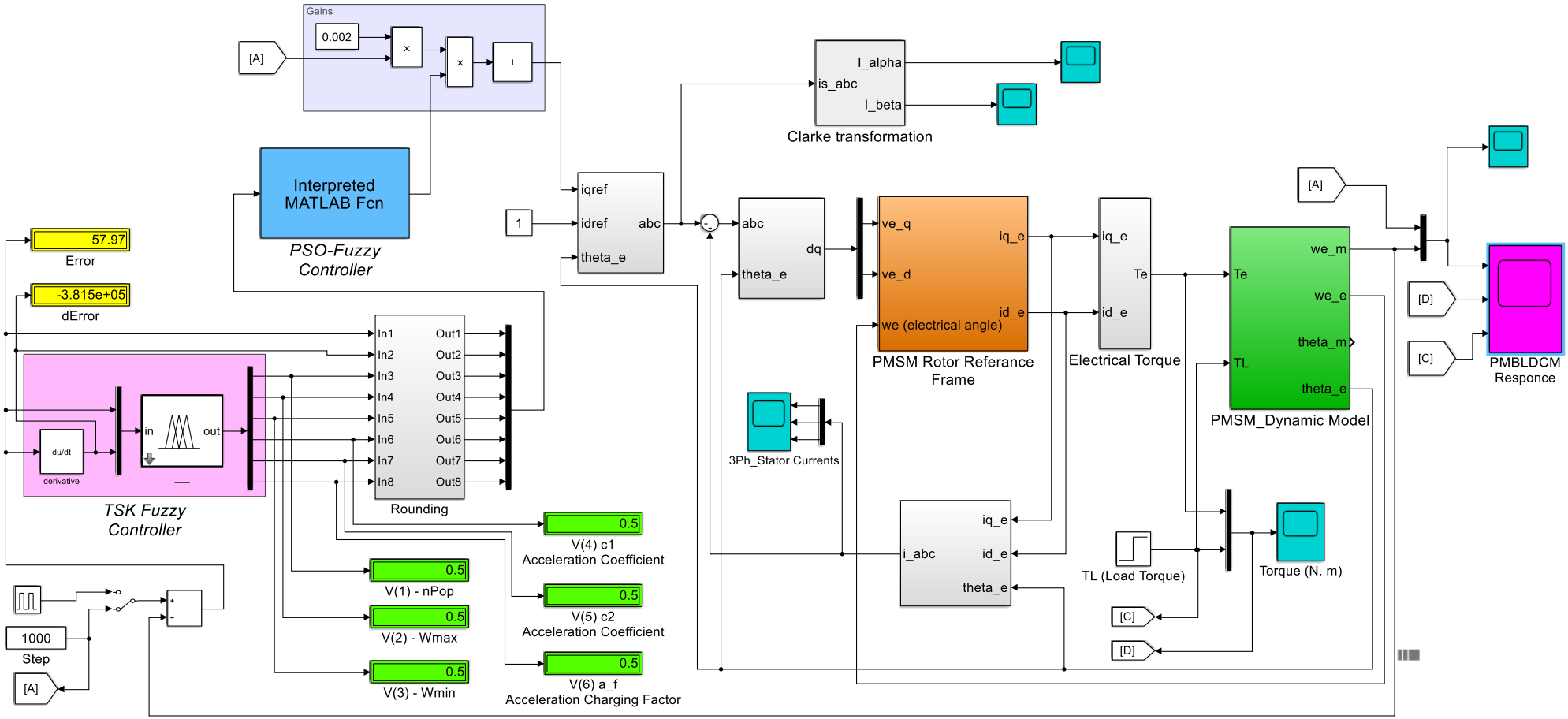

Fig. A.1. Overall Simulink model of the proposed TSK-PSO-FLC

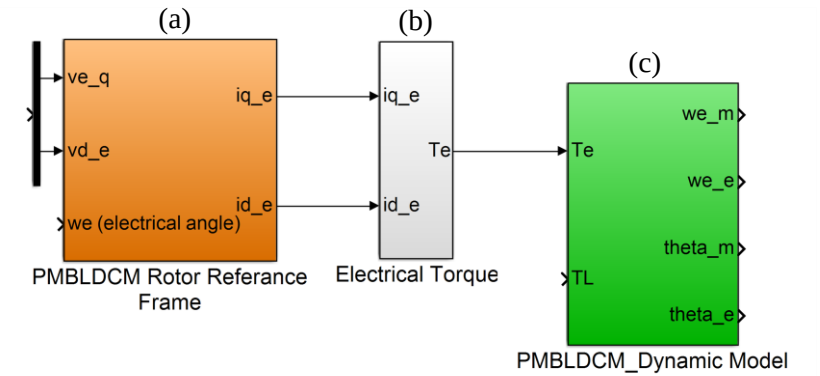

Fig. A.2. Extracted Simulink model of the rotor reference frame, electrical torque and the PMBLDC dynamic behaviour

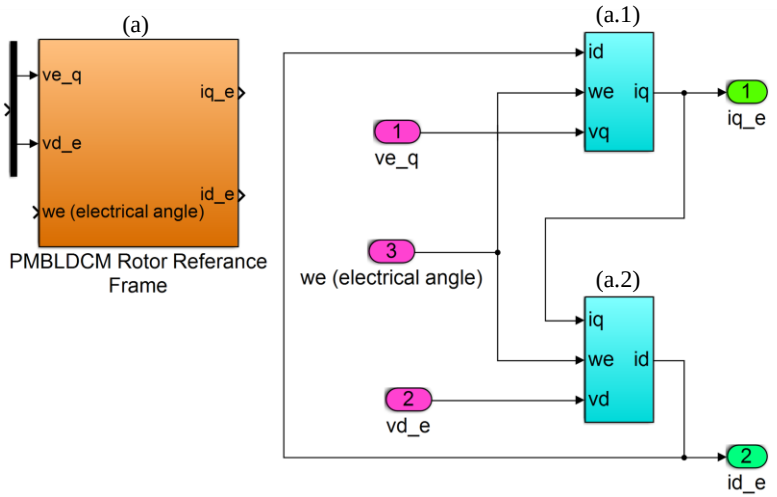

Fig. A.3. Extracted Simulink model of the rotor reference frame

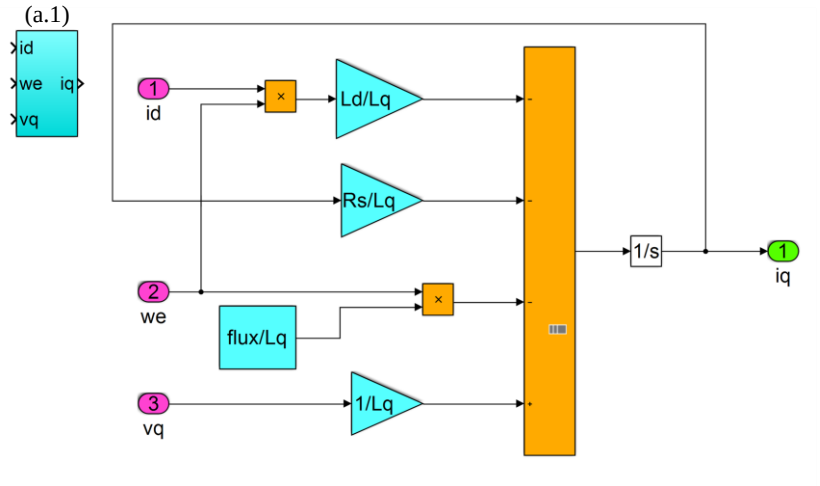

Fig. A.4. Extracted Simulink model of the rotor reference frame Part - I

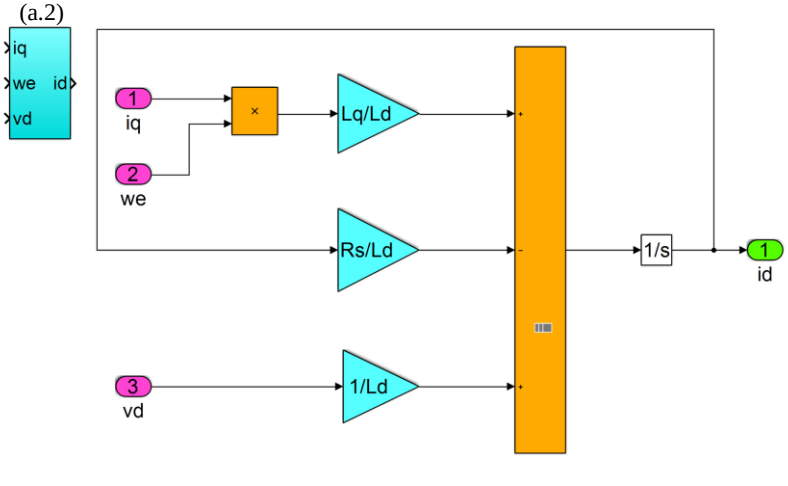

Fig. A.5. Extracted Simulink model of the rotor reference frame Part - II

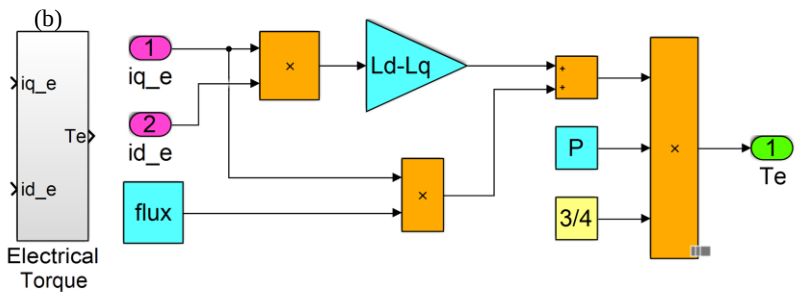

Fig. A.6. Extracted Simulink model of the electrical torque generator

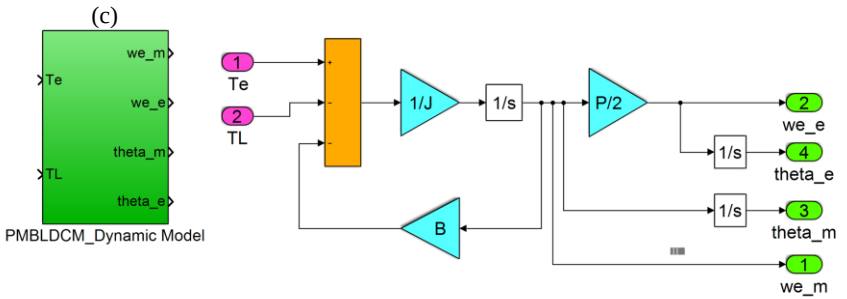

Fig. A.7. Extracted Simulink model of the PMBLDC motor dynamic behaviour

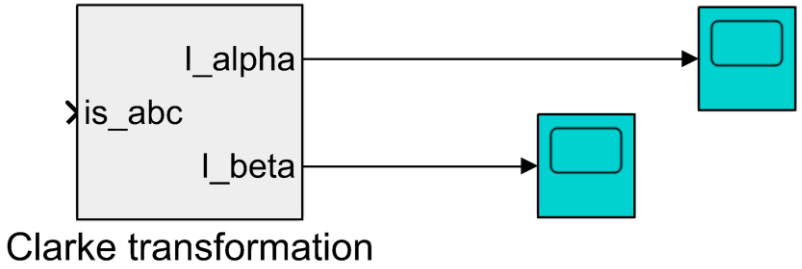

Fig. A.8. The 3-D stationary reference frame behaviour into a 2-D stationary reference frame

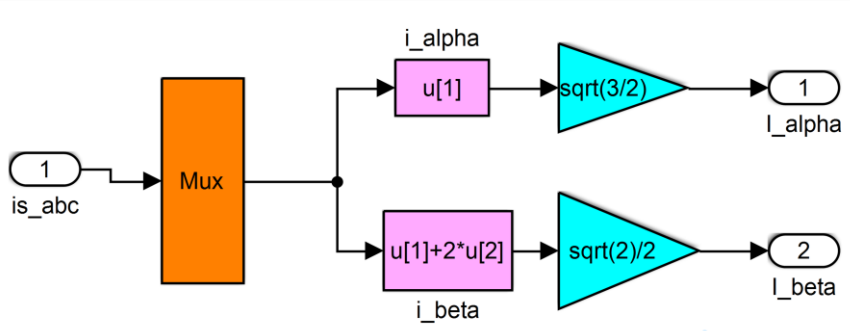

Fig. A.9. Extracted Simulink model of the 3-D stationary reference frame behaviour into a 2-D stationary reference frame

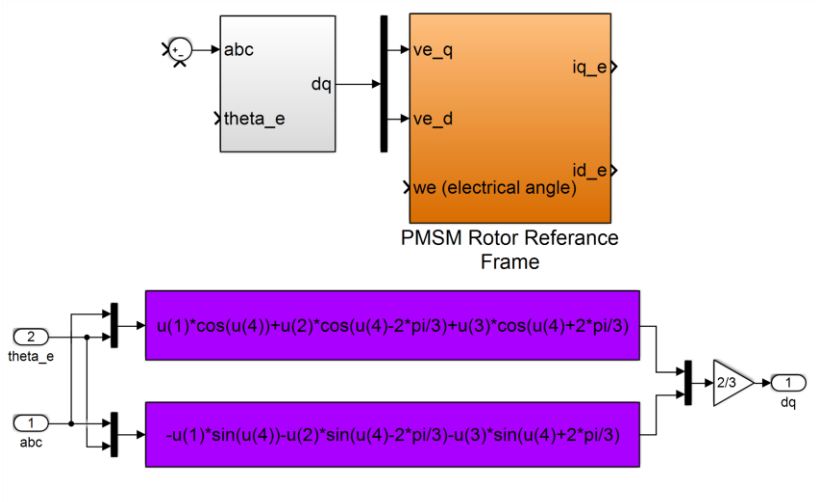

Fig. A.10. Extracted Simulink model of the 3-D stationary reference frame on to a 2-D rotating reference frame (*d-q* frame)

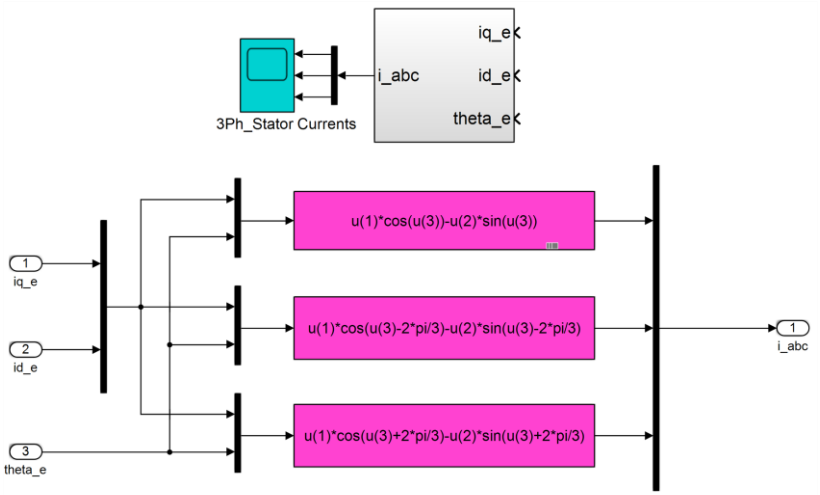

Fig. A.11. Extracted Simulink model of the stator 3-ph current conversion on to a 2-D rotating reference frame

Appendix – B

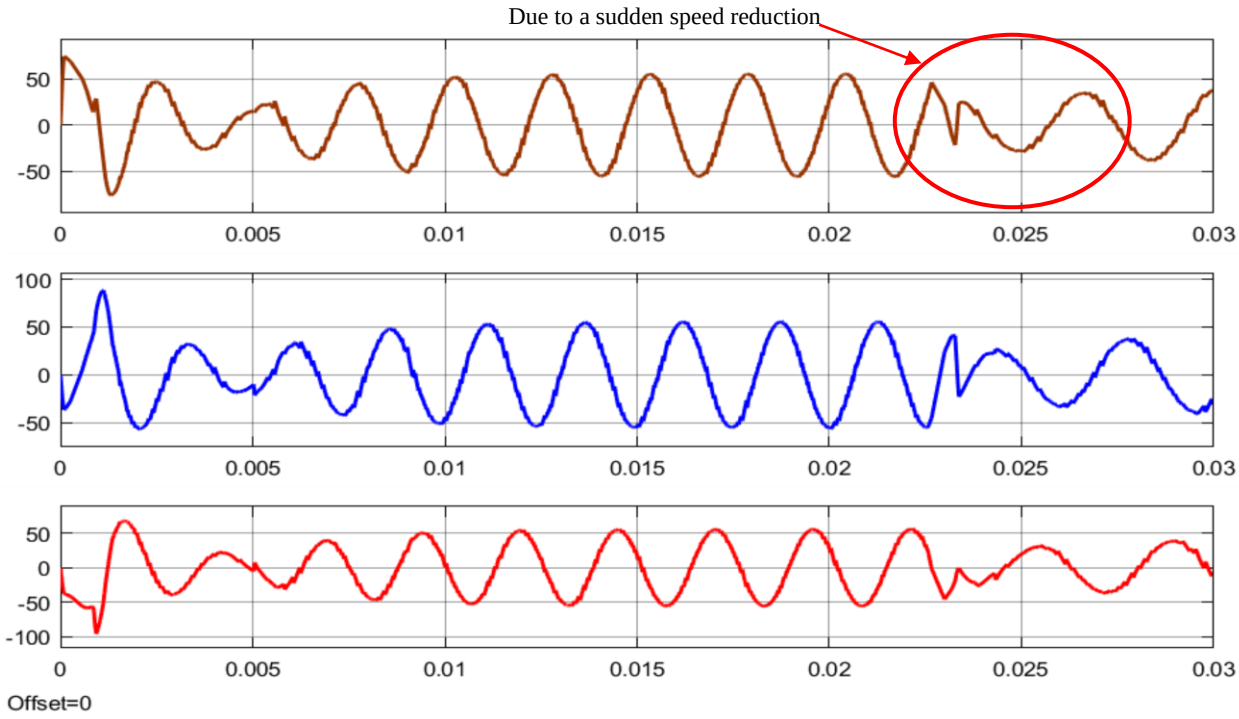

Fig. B.1. Stator current variation respect to the stationary (*a*-*b*-*c*) reference frame

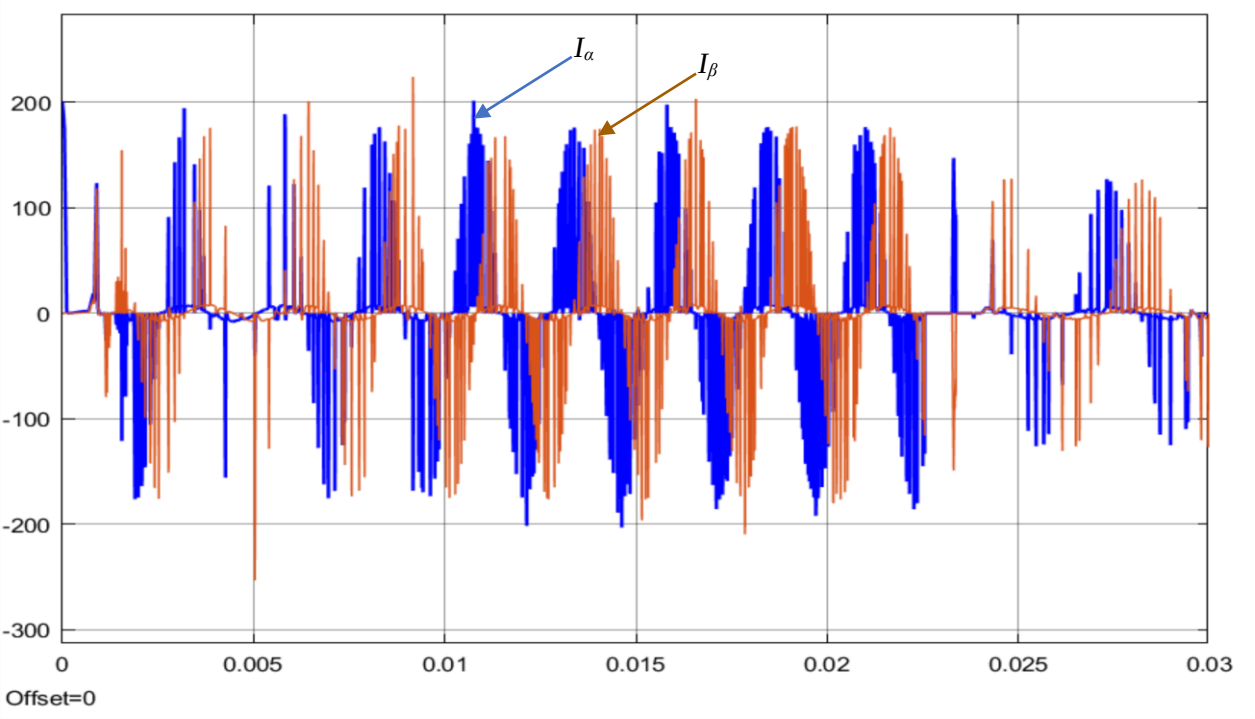

Fig. B.2. Stator current variation respect to the 2-D stationary reference frame (α, β - frame)

Appendix – C

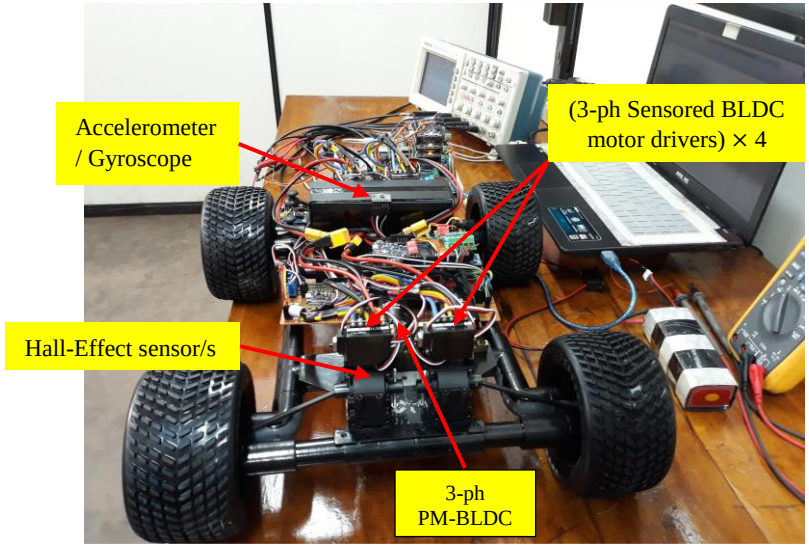

Fig. C.1. The designed and developed 4WD electric rover with the TSK-PSO-FLC

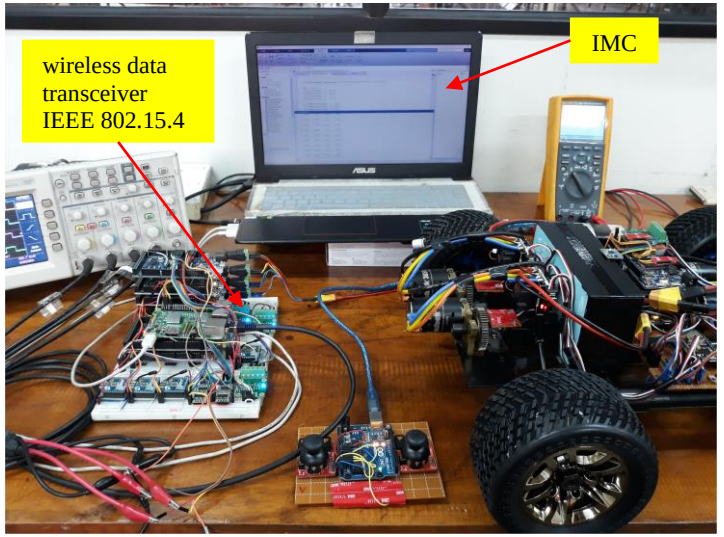

Fig. C.2. The developed wireless transceiver with a system database (up to 2 km)

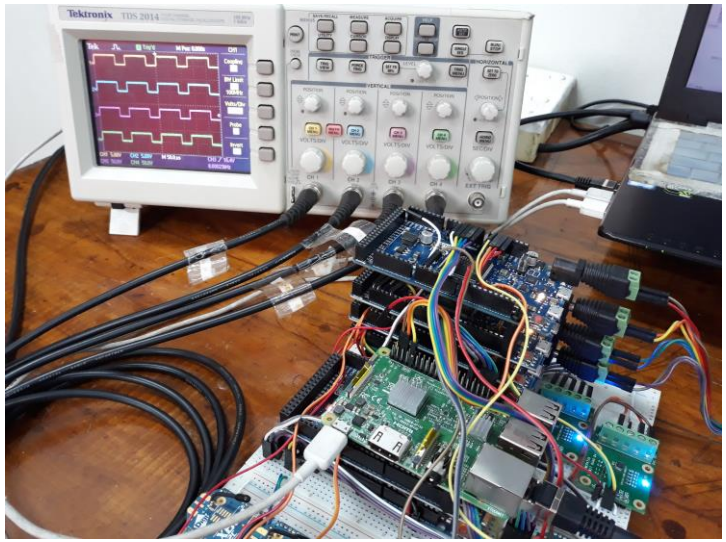

Fig. C.3. The synchronized four motor drive signal for every sampling instant "*k*"

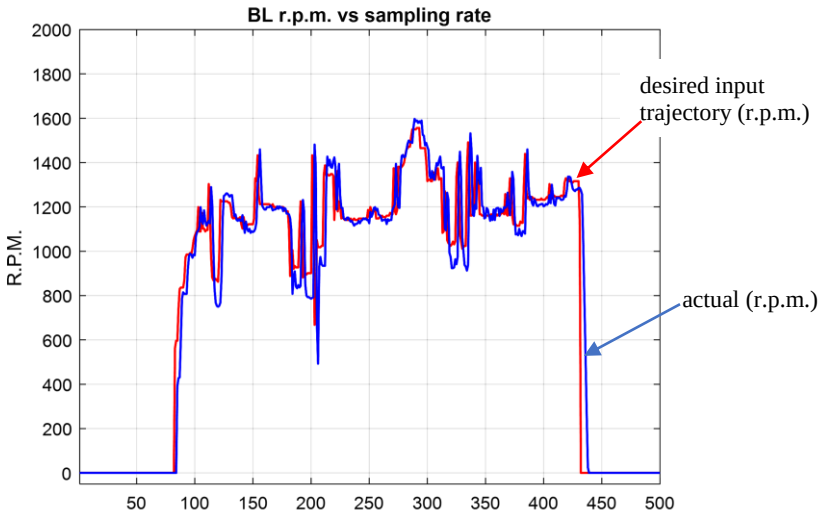

Fig. C.4. The back-left tire response for a desired input trajectory (50 samples /sec)

Acknowledgements

This work was supported by the Open University of Sri Lanka, Sri Lanka.

References

[1]. R. Souad, H. Zeroug, Comparison between direct torque control and vector control of a permanent magnet synchronous motor drive, *Proc. 13th IEEE Conf. on Power Electronics and Motion Control Conference (EPE-PEMC)* 2008, 1209-1214.

[2]. N. Jayamary Sujatha, M. Saravanan, A comparative study of fuzzy logic controllers for BLDC motor drive, *ARPN Journal of Engineering and Applied Sciences*, vol. 10, no. 9, 2015, 4167-4175.

[3]. E. Siqueira, J. Mor, R.Z. Azzolin, Algorithm to identification of parameters and automatic re-project of speed controller of BLDC motor, *International Federation of Automatic Control Hosting*, Elsevier Ltd, IFAC-Papers online 48-19, 2015, 256–261.

[4]. M. Tariq, T.K. Bhattacharya, N. Varshney, D. Rajapan, Fast response Antiwindup pi speed controller of brushless dc motor drive: modeling, simulation and implementation on DSP, *Journal of Electrical Systems and Information Technology*, vol. 3, 2016, 1–13.

[5]. A. El-samahy, M. Shamseldin, Brushless DC motor tracking control using self-tuning fuzzy PID control and model reference adaptive control, *Ain Shams Engineering Journal*, 2016, 1-12.

[6]. K. Premkumar, B.V. Manikandan, Bat algorithm optimized fuzzy PD based speed controller for brushless direct current motor, *Engineering Science and Technology, an International Journal* 19.2 2016, 818–840.

[7]. A. Rubaai, P. Young, Hardware/software implementation of fuzzy-neural network self-learning control methods for brushless dc motor drives, *Journal of IEEE Transactions on Industry Applications*, 2015, 1-12.

[8]. H.E.A. Ibrahim, F.N. Hassan, A.O. Shomer, Optimal PID control of a brushless DC motor using PSO and BF techniques, *Ain Shams Engineering Journal* 5, 2014, 391–398.

[9]. A.S. El-Wakeel, A.E.K.M. Ellissy, A.M. Abdel-hamed, A hybrid bacterial foraging-particle swarm optimization technique for optimal tuning of proportional-integral-derivative controller of a permanent magnet brushless DC motor, *Taylor & Francis Group, LLC, Electric Power Components and Systems*, 43(3), 2015, 309–319.

[10]. B.N. Kommula, V.R. Kota, Mathematical Modeling and Fuzzy Logic Control of a Brushless DC Motor Employed in Automobile and Industrial Applications, *Proc. 1st IEEE Conf. on Control, Measurement and Instrumentation (CMI)* 2016, 1-5.

[11]. G. Pavithra, G.R.P. Lakshmi, Simulation of neuro fuzzy and ANFIS in sensorless control of BLDCM drive for high speed application, *Proc. IEEE Conf. on Computation of Power, Energy, Information and Communication*, 2015, 306-312.

[12]. T.V. Kiran, N. Renuka Devi, Particle swarm optimization based direct torque control (DTC) of induction motor, *International Journal of Advanced Research in Electrical, Electronics and Instrumentation Engineering*, Vol. 2, Issue 7, July 2013, 3471-3476.

[13]. M. Milani, T. Cavdar, V.F. Aghjehkand, Particle swarm optimization-based determination of Ziegler Nichols parameters for PID controller of brushless dc motors, *Proc. IEEE Conf. on Innovations in Intelligent Systems and Applications (INISTA)*, 2012, 1-5.

[14]. H.R. Jayetileke, W.R. de Mel, H.U.W. Ratnayake, Modelling and simulation analysis of the genetic-fuzzy controller for speed regulation of a Sensored BLDC motor using Matlab/Simulink, *Proc. 13th IEEE Conf. on Industrial and Information Systems (ICIIS)*, 2017, 1-6.

[15]. R. Eberhart, J. Kennedy, A new optimizer using particle swarm theory, *Proc. 6th IEEE Conf. on Micro Machine and Human Science*, 1995, 39-43.

[16]. H.R. Jayetileke, W.R. de Mel, H.U.W. Ratnayake, Real-time fuzzy logic speed tracking controller for a dc motor using Arduino Due, *Proc. 7th IEEE Conf. on Information and Automation for Sustainability (ICIAfS)*, 2014, 1-6.

[17]. W. R. de Mel, A. N. Poo, Real-time control using xpc-target in Matlab, *International Symposium on Dynamics and Control, Hanoi, Vietnam*, 2003, 1-8.

[18]. H. Açikgöz, O.F. Keçecioglu, G.A. Ahmet, and M. Sekkeli, Speed control of direct torque-controlled induction motor by using PI, anti-windup PI and fuzzy logic controller, *International Journal of Intelligent Systems and Applications in Engineering*, 2(3), 2014, pp.58-63.

[19]. A. Uysal, Real-Time Fuzzy Logic Control of Switched Reluctance Motor, *International Journal of Intelligent Systems and Applications in Engineering*, 5(3), 2017, pp.135-139.

[20]. H. Acikgoz, Speed control of DC motor using interval type-2 fuzzy logic controller, *International Journal of Intelligent Systems and Applications in Engineering*, 6(3), 2018, pp.197-202.

[21]. B. Allaoua, B. Gasbaoui, B. Mebarki, setting up PID dc motor speed control alteration parameters using particle swarm optimization strategy, *Leonardo Electronic Journal of Practices and Technologies*, vol 14, 2009, 19-32.

[22]. M.M. Sabir, J.A. Khan, Optimal design of PID controller for the speed control of dc motor by using metaheuristic techniques, *Hindawi Journal of Advances in Artificial Neural Systems*, Vol. 2014, 2014, 1-8.

[23]. E.H.E. Bayoumi, Z.A. Salmeen, Practical swarm intelligent control brushless dc motor drive system using GSM technology, *Journal of WSEAS Transactions on Circuits and Systems*, Vol 13, 2014, 188-201.